Published in final edited form as:
Exp Cell Res. 2007 July 1; 313(11): 2465–2475.

Role of phosphatidylinositol-4-phosphate 5′ kinase (*ppk-1*) in ovulation of *Caenorhabditis elegans*

Xiaojian Xu[a], **Haisu Guo**[a], **Diane L. Wycuff**[b], and **Myeongwoo Lee**[a,*]

a *Department of Biology, Baylor University, One Bear Place 97388, Waco, TX 76798*

b *Molecular Bioscience Center, Baylor University, One Bear Place 97046, Waco, TX 76798*

Abstract

During *C. elegans* ovulation, the somatic gonad integrates signals from germ cells and propels a mature oocyte into the spermatheca for fertilization. Previous work suggests that phosphoinositide signaling plays important roles in *C. elegans* fertility. To fully understand inositol-1,4,5-trisphosphate (IP_3) signaling in ovulation, we have examined the function of phosphatidylinositol-4-phosphate 5′ kinase (PIP5K) in *C. elegans*. Our results show that the *C. elegans* PIP5K homolog, *ppk-1*, is essential for ovulation in *C. elegans; ppk-1* is mainly expressed in somatic gonad, and depletion of *ppk-1* expression causes defective ovulation, reduced gonad sheath contractility, and sterility. Increased IP_3 signaling compensates for *ppk-1 (RNAi)*-induced sterility, suggesting that *ppk-1* is linked to IP_3 signaling. These results demonstrate that *ppk-1* plays an essential role in IP_3 signaling and cytoskeleton organization in somatic gonad.

Keywords

gonad sheath; PIP5K; phosphoinositide; ovulation; myosin; IP_3; contraction; fertility; *ppk-1*; troponin

Introduction

The *C. elegans* gonad is composed of two U-shaped tubular gonad arms, connecting to the uterus in the ventral center of the animal. The distal gonad is filled with mitotic germ cells, which differentiate into sperm or oocytes. In contrast, germ cells in the proximal gonad undergo meiosis and become arrested at prophase I after oogenesis. In a process called oocyte maturation, the arrested oocyte will subsequently complete the rest of meiosis I to mature and achieve capability for fertilization [1–3]. General indications of oocyte maturation include nuclear envelope break down (NEBD) and oocyte cell rounding. The sperm-oocyte interaction is known to promote oocyte maturation. A major sperm protein (MSP) binds to VAB-1 on the oocyte surface by antagonizing the effect of VAB-1/Ephrin receptor (EphR) on the oocyte [4,5]. In contrast, MSP binds to VAB-1/EphR on gonad sheath cells and stimulates basal gonad contraction [4].

*All correspondence should be addressed to: Myeongwoo Lee, Ph.D., Tel) 254-710-2135, Fax) 254-710-2969, Email) myeongwoo_lee@baylor.edu..

During maturation, the proximal gonad rapidly contracts in response to signals from the maturing oocyte, reaching peak contraction levels concurrently with completion of oocyte maturation. As a result, the distal constriction (spermathecal valve) of the spermatheca dilates, allowing a mature oocyte to be propelled by contraction into the spermathecal lumen for fertilization, a process called ovulation [2]. Inositol-1,4,5-trisphosphate (IP_3) signaling plays essential roles in regulating sheath cell contraction during *C. elegans* ovulation [6–8]. The maturing oocyte secretes LIN-3/EGF to gonad sheath cells [9]. Upon binding of LIN-3/EGF to its receptors, sheath cells produce IP_3 by hydrolysis of phosphatidylinositol-4,5-bisphosphate (PIP_2), which is mediated by PLC-3/phospholipase Cγ. In turn, IP_3 binds to its receptor (IP_3R) on the surface of the ER, causing the release of intracellular calcium ions into the cytosol [6,7]. Released calcium ions then interact with other signaling molecules to control cellular organization and cytoskeletal assembly [10].

Phosphatidylinositol-4-phosphate 5′ kinase (PIP5K) is an essential kinase enzyme, phosphorylating the fifth hydroxyl of phosphatidylinositol-4-phosphate (PIP) to synthesize PIP_2, a signaling molecule that interacts with cytoskeleton regulatory proteins such as profilin, cofilin, and gelsolin [11]. Cells lacking PIP_2 generally display defective cytoskeleton organization that is similar to the phenotype observed after depletion of PIP5K [12]. In fact, mutations in *S. cerevisiae* Mss4/PIP5K results in defective actin cytoskeleton organization during polarized cell growth [13–15]. Studies on *skittles* (*sktl*) in *Drosophila* have revealed that *sktl*/PIP5K is required for cytoskeletal regulation during sensory structure development [16,17]. Biochemical analyses have also indicated that PIP5K interacts with Rho family GTPases to modulate actin cytoskeletal dynamics and organization, suggesting a role for PIP5K and PIP_2 in cytoskeletal organization [18,19].

The simple *C. elegans* gonad structure serves as a robust model system to explore the relationship between cytoskeleton organization and phosphoinositide signaling [3]. We report that depletion of *ppk-1*/PIP5K causes defective ovulation and gonad contractility, demonstrating that *ppk-1*/PIP5K is important for regulating cytoskeleton organization in *C. elegans* somatic gonad. We also have found that ITR-1/IP_3R mediates interaction between *ppk-1*/PIP5K and the cytoskeleton and have elucidated that UNC-54/myosin B is also responsive to *ppk-1 (RNAi)*.

Materials and Methods

Nematode and RNAi Analysis

All strains were maintained at room temperature (RT) on NGM agar seeded with *E. coli* OP50. The following strains used in this study were obtained from the Caenorhabditis Genetics Center, St. Paul, MN: wild-type N2, *lfe-2 (sy326)* I, *rrf-1(pk1417)* I, *itr-1 (sy290)* IV, *ipp-5 (sy605)* X, and *unc-54 (e190)* I.

For RNAi, N2 or mutant animals were cultured on RNAi plates, NGM agar supplemented with ampicillin (50 μg/ml) and β-lactose (0.02% w/v) and seeded with RNAi bacteria, *E. coli* HT115 (DE3). RNAi bacteria were cultured in Luria-Bertani (LB) broth, supplemented with ampicillin (50 μg/ml) before being seeded on RNAi plates. Plates were then incubated overnight at RT to induce the expression of dsRNA. Sterility and endomitotic (Emo) phenotypes of RNAi animals were examined using methods described in previous studies [8,20,21]. Well number I-2K18 of the *C. elegans* chromosome I RNAi library was the source of the *ppk-1 (RNAi)* bacterial clone. The individual bacterial clone was purchased from the UK HGMP Resources Center (Hinxton, UK). The plasmid from the bacterial clone was sequenced and verified to contain a *ppk-1* gene fragment.

GFP constructs

To generate a *ppk-1*::GFP reporter construct, nucleotide sequences upstream of the *ppk-1* gene (−2070 to +6, where +1 is the first base of ATG) were amplified from N2 genomic DNA using PCR and cloned into the *Sph*I and *Bam*HI sites of the GFP expression vector pPD95.77 (purchased from Addgene, CA). To generate a *ppk-1::pat-10::GFP* translation fusion construct, 1.1 kb (from ATG to TAA) of the nematode *pat-10* gene was amplified from N2 genomic DNA by PCR and cloned into a pGEM-T Vector (Promega, Madison, WI). Then *pat-10* (as a *Bgl*II - *Kpn*I fragment) and the *ppk-1* promoter (as a *Sph*I - *Bam*HI fragment) were cloned into the *Sph*I and *Kpn*I sites of GFP expression vector pPD95.77 to generate the *ppk-1::pat-10::GFP* construct.

A transgenic line, *kqEx51[ppk-1::gfp, pRF4],* carrying extrachromosomal arrays was generated by microinjecting 10 μg/ml of *ppk-1::GFP* into the gonad arm of adult N2 hermaphrodites along with 100 μg/ml of pRF4 [22], containing a dominant *rol-6 (su1006dm)* mutant gene, as a co-injection marker for transformation. A transgenic line, *kqEx61[ppk-1::pat-10::gfp, pRF4],* carrying extrachromosomal arrays to express *pat-10::GFP* translational fusion proteins was also generated similarly by microinjecting 50 μg/ml of *ppk-1::pat-10::GFP* with pRF4 (50 μg/ml).

In vivo analysis of sheath contraction and ovulation

Worms grown on *ppk-1* or *pPD129.36 (RNAi)* bacteria for 48 hours were collected in M9 buffer containing 0.1% tricaine and 0.01% tetramisole (w/v, Sigma-Aldrich Chem. Co, St. Louis, MO) for 30 min at RT [4]. When body movements stopped, animals were transferred onto 2% agarose pads and observed on a Nikon TE2000-U inverted microscope with a 40X Plan Fluor objective lens. Ovulation images were captured using a CoolSnap *cf* monochrome camera (Roper Scientific, CA) at RT and recorded every 15 s for 60–120 min using MetaVue (version 5) software. Time-lapse DIC images of the proximal gonad and oocytes were captured from the beginning of oocyte maturation, several minutes before the rounding of the first oocyte, to the entrance of the fertilized egg into the uterus. For *ppk-1 (RNAi)* animals, at least one hour of ovulation sequence was observed, and movies were generated from the beginning of oocyte maturation.

To measure the contractility of each gonad, ovulation sequences were captured using a CoolSnap *cf* monochrome camera in the video mode of RS Image software (version 1.6; Roper Scientific, Tucson, AZ) and recorded in an SSC-960 time-lapse VCR (Samsung Electronics, S. Korea), 72 hr record mode. To score the number of proximal gonad contractions, the video was played in 6 hr playback mode. Lateral displacement of the proximal gonad was scored as 'contraction.' Basal sheath contractions were counted for a 15-min interval before the onset of oocyte maturation. Contractions that occurred within one minute following oocyte maturation were scored as ovulatory sheath contractions.

Fluorescence microscopy of *C. elegans*

To visualize cytoskeletal organization in the gonad sheath, *ppk-1* or control RNAi treated worms were collected in M9 buffer containing 1% sodium azide (NaN_3, w/v). Using two 26-gauge needles, worms were decapitated and the gonad extruded [23,24]. These dissected gonads were placed on poly-L-lysine (1 mg/ml, w/v) coated slides and fixed with methanol and acetone at −20°C, followed by treatment with LS25, anti-UNC-54 monoclonal antibody ascites fluid (1:1,000 dilution in M9 buffer with 1% goat serum) [25,26], overnight at RT. The samples were then treated with a secondary goat anti-mouse IgG FITC conjugated antibody, (Sigma-Aldrich Chem. Co., St. Louis, MO) (1:10,000 dilution in M9 buffer with 1% goat serum), for 2–3 hrs at RT. The samples were washed and mounted on a Nikon TE2000-U inverted microscope for fluorescence microscopy. To observe the distribution of PAT-10 in

the gonad, *kqEx61* animals were anesthetized in M9 buffer containing 1% (w/v) sodium azide, and their gonads were extruded with 26-gauge syringe needles. Dissected gonads were mounted on 2% agarose pads and observed on the Nikon TE2000-U inverted microscope. Images were captured using a CoolSnap *cf* monochrome camera (Roper Scientific, Tucson, AZ) and analyzed with Metavue imaging software (version 5, Molecular Devices Co, Downingtown, PA).

RESULTS

Expression pattern and RNA interference (RNAi) phenotype of ppk-1

In order to identify the tissues where *ppk-1* is localized, we examined its expression pattern in *C. elegans*. A *ppk-1*::GFP transcriptional reporter construct (see Materials and Methods) was microinjected into wild-type *C. elegans*, and transgenic lines expressing *ppk-1*::GFP were generated. *ppk-1::GFP* expression was observed in such somatic tissues as gonad sheath (Figure 1F) and spermatheca (Figure 1D), distal tip cells (Figure 1B), and uterine and vulva muscles (Figure 1D). *ppk-1*::GFP also showed extensive expression in such neuronal cells as ventral nerve cord (Figure 1C), neuronal cell bodies near the nerve ring, and tail neurons (data not shown).

To investigate the role of IP_3 signaling in fertility, *ppk-1*/PIP5K expression [27,28] was depleted in postembryonic wild-type *C. elegans* by RNAi. Ninety three percent of *ppk-1 (RNAi)* animals produced no progeny (n=100) (Table 1). Since the observed sterility phenotype of *ppk-1 (RNAi)* animals could result either from defective germ cell development or structural defects in the somatic gonad, we repeated the RNAi experiment in the background of the *rrf-1 (pk1417)* allele, which carries a mutation that inhibits RNAi in somatic cells, but not the germline [29]. In the *rrf-1 (pk1417)* background, the *ppk-1 (RNAi)* phenotype is significantly reduced (n=55) (Table 1), suggesting that *ppk-1 (RNAi)* causes defects in soma. Additionally, we found additional PIP5K homologs, *ppk-2* and *ppk-3* from a Wormbase search [30,31]. However, RNAi of *ppk-2* or *ppk-3* failed to show overt fertility defects (data not shown).

ppk-1 is essential for proximal gonad contractility

Previous work has suggested that decreased IP_3 signaling causes defective ovulation by reducing proximal gonad contractility during ovulation [7,8,32]. Thus, we reasoned that loss of *ppk-1*/PIP5K expression might inhibit proximal gonad contractility by decreasing IP_3 synthesis. *C. elegans* gonad alternates between two contractile modes in the sheath: 1) ovulatory contraction: increased and accelerating contractile activity triggered by oocyte maturation, and 2) basal contraction: constitutive contractile activity between ovulations. Gonad sheath routinely contracts at the basal rate but contractions increase to ovulatory rates during oocyte maturation and reach peak activity right before ovulation. Increased contractile activity returns to basal levels after ovulation is completed, suggesting that oocyte maturation is required for triggering ovulatory contraction of gonad sheath [2].

In order to define the role of *ppk-1* in gonad contraction, ovulation of *ppk-1 (RNAi)* animals was monitored by time-lapse differential interference contrast (DIC) microscopy [21,33]. In all control RNAi worms monitored, the proximal oocyte underwent maturation, marked by NEBD and cell rounding (Table 2) [1,2,4,5]. Maturation was followed by dilation of the spermathecal valve then by the entrance of the matured oocyte into the spermatheca for fertilization (Movie 1, Figure 2A–D). During this process, mean basal and ovulatory sheath contraction rates of control RNAi were scored at 8.5 ± 0.46 (n=5) and 16.2 ± 0.72 (n=5) contractions/min, respectively (Figure 3).

In all *ppk-1 (RNAi)* worms examined, the proximal oocyte completed typical maturation processes, including nuclear disappearance and cortical rearrangement (cell rounding) [1,2] (Table 2). However, neither intense contraction of gonad sheath nor dilation of the spermathecal valve occurred during maturation (Table 2). Instead, due to defective somatic gonad contraction, matured oocytes were trapped in the proximal gonad with no propulsion into the spermatheca. Trapped oocytes appeared to regain nuclear morphology and undergo several rounds of incomplete cell division (Movie 2, Figure 2E–H). In extended observations, the second and third oocytes continued to proceed through the maturation process, demonstrating that *ppk-1 (RNAi)* caused defects in somatic gonad contractile capability, but did not affect oocyte maturation *per se* (Table 2). Mean basal and ovulatory contraction rates of *ppk-1 (RNAi)* gonad were measured at 4.8 ± 0.23 (n=6) and 6 ± 0.55 (n=5) contractions/min (Figure 3), suggesting that *ppk-1 (RNAi)* significantly reduced the contractility of the proximal gonad in both contraction modes.

Genetic interaction of ppk-1

PPK-1/PIP5K is an enzyme that phosphorylates phosphatidylinositol-4-phosphate on the cell membrane inner leaflet to yield phosphatidylinositol-4,5-bisphosphate (PIP_2) [27,28]. PIP_2 in turn further reacts with phospholipase C (PLC) or phosphatidylinositol-3 kinase (PI-3-kinase). Particularly, PLC hydrolyzes PIP_2 into IP_3 and diacylglycerol. IP_3 binds to IP_3 receptor (*itr-1*/IP_3R) on the ER surface and triggers release of intracellular calcium ions into the cytosol [34–36]. We previously reported that increased IP_3 signaling mutants such as gain-of-function (*gf*) *itr-1*/IP_3R, reduction-of-function (*rf*) *lfe-2*/IP_3K [6], and loss-of-function (*lf*) *ipp-5*/type I 5′ phosphatase [9] were able to suppress the sterility of *pat-3*/integrin β or *plc-3/PLCγ (RNAi)* [8].

To test whether *ppk-1* is also linked to IP_3 signaling, we performed *ppk-1 (RNAi)* in increased IP_3 signaling backgrounds. We used a gain-of-function *(gf)* allele of *itr-1 (sy290)* carrying a missense mutation in the IP_3 binding domain of ITR-1/IP_3R [6]. The *ppk-1 (RNAi)* displayed 2.5% (n= 77) sterility in the *itr-1* (*sy290)* background, whereas the percentage of sterility was higher in *lfe-2 (sy326)* or *ipp-5 (sy605)* backgrounds, 75% (n=60) and 62 % (n=50), respectively (Table 1). These data indicate that *ppk-1* (RNAi) sterility was virtually completely suppressed by the gain-of-function *itr-1*, whereas the removal of *lfe-2* and *ipp-5* partially suppressed *ppk-1 (RNAi)* sterility (Table 1). Moreover, ovulation monitoring of *ipp-5 (sy605); ppk-1 (RNAi)* animals by time-lapse DIC video microscopy revealed a relatively low percentage of defective ovulation (33%, n=6). In accordance with the sterility data, ovulation defects resulting from *ppk-1 (RNAi)* were suppressed incompletely in *ipp-5 (sy605)* (Table 2). To verify *ppk-1* depletion in the *itr-1 (sy290)* background, reverse transcription PCR (RT-PCR) was performed, and the level of *ppk-1* expression was assessed. In *itr-1 (sy290); ppk-1 (RNAi)* animals, similar to the *ppk-1 (RNAi)* in N2 background worms, *ppk-1* expression was significantly decreased (Figure S1). Taken together, these data demonstrate that gain-of-function IP_3R activity can overcome the effect of *ppk-1* depletion and that *itr-1* is a downstream effector of *ppk-1*.

To investigate whether *itr-1 (gf)* suppression of the *ppk-1 (RNAi)* fertility defect correlates with suppression of *ppk-1 (RNAi)* contractility defects, basal and ovulatory contraction rates of *ppk-1 (RNAi)* in the *itr-1 (gf)* background were assessed using time-lapse DIC video microscopy (Table 2). Like the fertility defects, reduced contractility of *ppk-1 (RNAi)* was also suppressed in the *itr-1 (sy290)* background. In all *itr-1 (sy290); ppk-1 (RNAi)* worms, no abnormality in maturation or ovulation was observed (Table 2). Dilation of the spermathecal valve and oocyte entrance into the spermatheca appeared normal as compared to control RNAi (Movie 3, Figure 2M–P). Mean basal and ovulatory levels of control RNAi in the *itr-1 (sy290)* background were scored at 7.2 ± 0.13 (n=5) and 10.8 ± 0.46 (n=5) contractions/min

(Figure 2I–L), whereas basal and ovulatory contraction rates in *ppk-1 (RNAi)* animals were scored at 6.8 ± 0.25 (n=5) and 13.5 ± 0.82 (n=5) contractions/min (Figure 3), respectively. These data demonstrate that *ppk-1* also influences gonad contractility via activity of ITR-1/ IP_3R.

ppk-1 (RNAi) causes Emo phenotype in oocytes and cytoskeletal defects in the proximal gonad

In *C. elegans*, the proximal gonad contains developing oocytes, which are arranged in a linear sequence of advancing stages of oogenesis as they move closer to the spermatheca [1,2]. Control RNAi animals showed a typical assembly line pattern of developing oocytes in a linear arrangement in the proximal gonad (Figure 4A). In contrast, the proximal gonad of *ppk-1 (RNAi)* animals showed no such regular arrangement (Figure 4C). Oocytes accumulated and piled on top of each other in the proximal gonad. In order to characterize gonad morphological defects in these worms, *ppk-1 (RNAi)* animals were stained with 4′,6-diamidino-2-phenylindole (DAPI) to visualize the nuclear morphology of accumulated oocytes (Figure 4B, D, and F) [23]. In all *ppk-1 (RNAi)* animals, proximal gonads displayed large clumps of DNA staining, which is indicative of endomitotic nuclei (Emo) (Figure 4C and D) (Table 2). Defective ovulation resulted in the Emo phenotype, due to failure of oocytes to proceed into the spermatheca for fertilization [20,26,37]. Sperm nuclei were located in the area proximal to the vulva and did not appear to overlap with the Emo oocytes (Figures 4D and 5C), suggesting that these oocytes are accumulated in the proximal gonad rather than in the spermatheca.

The reduced contractility (Figure 3) and Emo appearance (Figure 4C and D) of *ppk-1 (RNAi)* animals led us to investigate proximal gonad contractile machinery. Sheath cells, a group of contractile myoepithelial cells with non-striated and randomly distributed actomyosin filaments, comprise the proximal gonad tube structure [38]. *ppk-1 (RNAi)* worms were stained with anti-UNC-54/myosin B monoclonal antibody [25,39,40] to visualize myosin filaments in the proximal gonad (Figure 5A and B). In contrast to control RNAi animals, which displayed evenly distributed myosin filaments in the proximal gonad, the myosin filaments of *ppk-1 (RNAi)* animals appeared fewer in number and disorganized (Figure 5C and D), suggesting that *ppk-1* is required for organization of myosin filaments in the gonad sheath or that an abnormal myosin expression pattern likely contributes to the observed defective phenotype.

One explanation of a requirement for *ppk-1* in UNC-54 organization is that accumulation of Emo oocytes in the proximal gonad promotes mechanical damage to the sheath cells, resulting in the myosin disorganization. To address this possibility, we examined the UNC-54/myosin B distribution patterns in non-Emo gonads from RNAi L4 larvae or young adults, a developmental stage at which such mechanical damage would presumably have not yet occurred. Although the gonads did not exhibit an Emo phenotype, UNC-54/myosin B filaments in these *ppk-1 (RNAi)* animals appeared to be less organized than in the control RNAi (Figure 5E and F), albeit with a lesser degree of disorganization than that seen in the Emo phenotype worms (Figure 5C and D). Compared to the gonad of control RNAi worms in Figure 5B, these gonads contained filaments which were more randomly organized (Figure 5F). To examine actomyosin filament organization further, a construct containing a PAT-10/troponin::GFP fusion under control of a *ppk-1* promoter was used to express protein in gonad sheath and GFP expression was examined. PAT-10/troponin C is a calcium binding protein that interacts with myosin filaments and is expressed in body wall muscle and gonad sheath cells [33, 41]. In control RNAi worms, the distribution of PAT-10::GFP protein in the sheath was similar to the UNC-54 distribution of control RNAi animals in N2 background (Figure 5B and I). By contrast, in *ppk-1 (RNAi)*, the proximal gonad showed a less well-organized PAT-10::GFP distribution pattern (Figure 5J), indicating that *ppk-1 (RNAi)* resulted in cytoskeleton disorganization in

sheath cells prior to the onset of Emo defects and presumably prior to any resultant possible mechanical damage to the gonad sheath.

Since we have demonstrated that both sterility and gonad contractility resulting from *ppk-1 (RNAi)* (Table 1, Figures 2 and 3) are suppressed by the *itr-1 (gf)* mutation, we also investigated the consequence of this genetic interaction to gonad morphology (Figures 4 and 5). In *itr-1 (gf); ppk-1 (RNAi)* worms, oocyte arrangements in the proximal gonad appeared normal as compared to the control RNAi. The proximal gonad displayed the typical linear arrangement of oocytes with graded development (Figure 4E and F) in both RNAi conditions. To examine whether the *itr-1* mutation also rescued the UNC-54/myosin B filament disorganization phenotype, *ppk-1 (RNAi)* was performed in the *itr-1 (sy290)* background. Animals were stained with anti-UNC-54/myosin B antibodies and examined by fluorescence microscopy. Concordant with the gonad morphology results, staining patterns of UNC-54/myosin B also appeared normal in *itr-1 (sy290)* animals, with either the control or the *ppk-1 (RNAi)* (Figure 5G and H), confirming that PPK-1 regulates cytoskeleton organization of myoepithelial gonad sheath via ITR-1/IP_3R.

ppk-1 is related to the function of UNC-54/myosin B

A role for UNC-54/myosin B in ovulation has been reported previously [42]. In that study, *unc-54 (e190)*, a null allele of *unc-54*, resulted in weaker sheath contraction than wild-type. The disruption of UNC-54/myosin B organization in *ppk-1 (RNAi)* prompted us to assess the effect of *ppk-1* depletion in an *unc-54 (e190)* background.

In the control RNAi, *unc-54 (e190)* animals appeared to have significantly reduced proximal gonad contractility with a basal rate of 2.13 ± 0.2 contractions/min (n=6) and an ovulatory rate of 5.25 ± 0.4 contractions/min (n=6) (Figure 3). Although 33% (n=6) of these animals exhibited defective ovulation, the proximal oocyte underwent maturation and ovulation (Table 2). To assess genetic interaction, *ppk-1* expression was depleted in the *unc-54 (e190)* background. *unc-54 (e190); ppk-1 (RNAi)* animals had similar basal and ovulatory sheath contraction rates to those of the control *unc-54 (e190)* animals, a basal rate of 2.29 ± 0.12 (n=5) and an ovulatory rate of 5.33 ± 0.21 (n=5). The similar sheath contraction rate of *ppk-1* and control RNAi animals within the context of the *unc-54 (e190)* background suggest that *ppk-1* activity is linked to *unc-54* in *C. elegans* sheath cell contractility.

DISCUSSION

Our results demonstrate that *ppk-1* expression is essential for ovulation of *C. elegans*. Although *ppk-1* expression was seen in neuronal tissues, we found *ppk-1* expression in such somatic tissues as gonad sheath, distal tip cells, spermatheca, and uterine and vulva muscles (Figure 1), indicating that it likely plays a major role in gonad activities. Functional studies of *ppk-1* revealed that depletion of *ppk-1* expression caused sterility (Table 1), defective ovulation (Figures 2 and 4, Table 2), reduced contractility of the gonad sheath (Figure 3), and disrupted myosin filament organization (Figure 5). In addition, this study reports that *ppk-1* is genetically linked to *itr-1* and *unc-54* (Figures 2 and 3, Table 1), suggesting that *ppk-1* may play an important role in calcium signaling and that *ppk-1* is connected to the function of *unc-54*/ myosin B, contributing to cytoskeletal organization in the gonad sheath.

PPK-1 is linked to IP_3 signaling

PPK-1/PIP5K is an enzyme which converts phosphatidylinositol-4-phosphate (PIP) into phosphatidylinositol-4,5-bisphosphate (PIP_2) on the cell membrane. PIP_2 is essential for proper formation of the cellular actin cytoskeleton [10,43]. Reduced PPK-1 results in depleted PIP_2. Lack of PIP_2 in turn halts production of IP_3, consequently lowering intracellular calcium ion

concentrations as a result of greatly reduced IP_3 binding to ITR-1/IP_3R on ER. Our data showing the genetic interactions of *ppk-1* are consonant with the biochemical function of *ppk-1*/PIP5K.

ppk-1 (RNAi)-induced sterility was suppressed in the *itr-1(sy290)* background (Tables 1 and 2). The mutation in *sy290* is a gain-of-function that makes ITR-1/IP_3R constitutively active or more sensitive to IP_3 molecules than wild type [6]. Suppression of sterility by *itr-1 (sy290)* confirms that IP_3 increased the activity of ITR-1/IP_3R. Depletion of *ppk-1* removes or significantly reduces PIP_2 levels. The lack of PIP_2 downregulates many downstream signaling events, including IP_3 production and activation of other phosphoinositides. The fact that *itr-1 (sy290)* is a gain-of-function mutation that causes calcium ion release leads us to suggest that the increased intracellular calcium level is responsible for reversion of the sterility phenotype of *ppk-1 (RNAi)* in the *itr-1 (sy290)* background. Calcium released from the smooth ER almost certainly promotes an elevated cytoplasmic calcium concentration, which is mediated by active ITR-1/IP_3R. The increased calcium most likely contributes to gonad sheath contractions during ovulation.

RNAi in a background of *lfe-2* or *ipp-5* loss-of-function alleles partially suppressed *ppk-1 (RNAi)* phenotypes (Tables 1 and 2). LFE-2 and IPP-5 are negative regulators of IP_3, and the removal of such negative regulators serves to increase IP_3 levels [6,9]. In *ppk-1 (RNAi)*, the level of PIP_2 has presumably been significantly decreased. Thus, the *lfe-2* or *ipp-5* mutation, under conditions of *ppk-1 (RNAi)*, may not result in adequate levels of IP_3 to stimulate the full release of intracellular calcium ions. An alternative explanation for the partial nature of the phenotype suppression may be that *lfe-2* and *ipp-5* are expressed and functional only in the spermatheca, whereas *ppk-1* is functional in both gonad sheath and spermatheca. The expression of *lfe-2* and *ipp-5* has been confined specifically to the spermatheca [6,9], whereas we find *ppk-1* is expressed both in the spermatheca and other parts of the somatic gonad. Perhaps, in the spermatheca, loss-of-function *lfe-2* or *ipp-5* results in sufficient IP_3 levels to stimulate calcium release to repress *ppk-1 (RNAi)* sterility phenotypes.

PPK-1 is important for organization of UNC-54/myosin B in gonad sheath

Our data also indicate that *ppk-1* is important for cytoskeleton organization in the gonad sheath (Figure 5). Dissected gonads of *ppk-1 (RNAi)* animals displayed disorganized and patchy distribution of UNC-54/myosin B, suggesting that IP_3 signaling contributes to actomyosin organization. Subsequent genetic analysis revealed that *ppk-1 (RNAi)* did not reduce gonad contractility within the *unc-54 (e190)* background, suggesting that *unc-54* may be epistatic to *ppk-1* (Figure 3). It is unlikely, however, that *ppk-1* and UNC-54/myosin B physically interact. Based on our data, it is reasonable to speculate that the interaction between *ppk-1* and UNC-54/myosin B may be mediated by ITR-1, supported by the suppression of *ppk-1 (RNAi)* phenotypes in the *itr-1 (gf)* background (Figures 2 and 3, Tables 1 and 2). Walker et al. (2002) have shown that ITR-1 directly interacts with myosin II, and this interaction is important for localized activation of IP_3-induced calcium signaling in the cell [44]. In addition, our preliminary results show that *unc-54 (RNAi)* in the *itr-1 (sy290)* background results in a sterile phenotype (Xu and Lee, unpublished data), suggesting that UNC-54/myosin B should be placed downstream of ITR-1. We cannot, however, rule out the possibility that MYO-3, a major skeletal myosin protein and known to be expressed in the proximal gonad [42,45], was also inactivated in the observed *unc-54 (RNAi)* phenotype.

In contrast to wild type worms, *ppk-1 (RNAi)* animals in the *unc-54 (e190)* background were sterile (Table 1), accumulated Emo oocytes in the proximal gonad, and evidenced no dilation of the spermathecal valve upon oocyte maturation, suggesting that the role of UNC-54 in the spermatheca is different from that in gonad sheath. In wild type gonad, contraction of sheath cells depends on IP_3 activity in response to LIN-3/EGF signals [7]. In turn, increased IP_3 levels

promote UNC-54/myosin B organization during gonad contraction. Interestingly, although localization experiments have detected UNC-54/myosin B in the gonad sheath, none has been identified in the spermatheca [1,46], suggesting that dilation of the spermathecal valve is independent of UNC-54/myosin B. Aono et al. (2002) have shown that RNAi of *par-3*, *par-6*, or *pkc-3* causes an Emo phenotype and absence of spermathecal dilation. The *par-3 (RNAi)* defects were partially suppressed by *ipp-5 (sy605)* [47]. They suggest that a PAR-3/PAR-6/PKC-3 complex may be involved in dilation of the spermatheca along with formation of spermathecal cell polarity. We suggest that, in the absence of UNC-54/myosin B, one or more myosin family members other than UNC-54 [48–50] may be linked to IP_3 signaling in the spermatheca.

How does IP_3 signaling regulate myosin organization?

This study has demonstrated that *ppk-1* is linked to *itr-1* and *unc-54*, suggesting that ITR-1/IP_3R mediates IP_3 signaling to regulate cytoskeleton organization in the gonad. ITR-1 is implicated in upregulated intracellular calcium levels in response to IP_3 as well as interactions with myosin II molecules [6,7,44,51]. It is unknown how ITR-1/IP_3R modulates UNC-54/myosin B organization in the gonad sheath. Our data suggest possible actions of ITR-1 in actomyosin organization. For example, ITR-1 may physically interact with UNC-54/myosin B to promote proper organization of myosin filaments [44]. However, additional experiments are required to elucidate the nature of the interaction between ITR-1 and UNC-54/myosin B within the context of gonad contraction and ovulation. Alternatively, effects of increased calcium ion concentration downstream of *itr-1* may result in the activities of calcium binding proteins such as troponins [52,53], tropomyosin [54], or myosin light chain kinase [55,56]. Ono and Ono (2004) demonstrated that *pat-10*/troponin C *(RNAi)* caused ovulation defects and cytoskeletal disorganization in the somatic gonad [33]. Our previous analyses have shown that *itr-1 (gf)* fails to suppress the sterility phenotype of *pat-10 (RNAi)*, suggesting that PAT-10/troponin C [53] may be a downstream effector of *itr-1* to regulate cytoskeletal organization in somatic gonad.

Taken together, our data have shown that *ppk-1* plays essential roles in *C. elegans* ovulation and that PPK-1/PIP5K interacts genetically with ITR-1/IP_3R and UNC-54/myosin B, demonstrating that control of contractions in the gonad occurs via IP_3 signaling.

Supplementary Material

Refer to Web version on PubMed Central for supplementary material.

Acknowledgements

C. elegans strains were provided by the Caenorhabditis Genetics Center, which is funded by the NIH. Authors thank Dr. Erin Cram at Northeastern University for her comments on our manuscript. This work was supported by funds from Faculty Research Initiative Program at Baylor University and a research grant from NIH (GM077156).

References

1. McCarter J, Bartlett B, Dang T, Schedl T. Soma-germ cell interactions in *Caenorhabditis elegans*: multiple events of hermaphrodite germline development require the somatic sheath and spermathecal lineages. Dev Biol 1997;181:121–143. [PubMed: 9013925]
2. McCarter J, Bartlett B, Dang T, Schedl T. On the control of oocyte meiotic maturation and ovulation in *Caenorhabditis elegans*. Dev Biol 1999;205:111–128. [PubMed: 9882501]
3. Hubbard EJ, Greenstein D. The *Caenorhabditis elegans* gonad: a test tube for cell and developmental biology. Dev Dyn 2000;218:2–22. [PubMed: 10822256]

4. Miller MA, Nguyen VQ, Lee MH, Kosinski M, Schedl T, Caprioli RM, Greenstein D. A sperm cytoskeletal protein that signals oocyte meiotic maturation and ovulation. Science 2001;291:2144–2147. [PubMed: 11251118]
5. Miller MA, Ruest PJ, Kosinski M, Hanks SK, Greenstein D. An Eph receptor sperm-sensing control mechanism for oocyte meiotic maturation in *Caenorhabditis elegans*. Genes Dev 2003;17:187–200. [PubMed: 12533508]
6. Clandinin TR, DeModena JA, Sternberg PW. Inositol trisphosphate mediates a RAS-independent response to LET-23 receptor tyrosine kinase activation in *C. elegans*. Cell 1998;92:523–533. [PubMed: 9491893]
7. Yin X, Gower NJ, Baylis HA, Strange K. IP3 signaling regulates rhythmic contractile activity of myoepithelial sheath cells in *C. elegans*. Mol Biol Cell 2004;15:3938–3949. [PubMed: 15194811]
8. Xu X, Lee D, Shih HY, Seo S, Ahn J, Lee M. Linking integrin to IP(3) signaling is important for ovulation in *Caenorhabditis elegans*. FEBS Lett 2005;579:549–553. [PubMed: 15642374]
9. Bui YK, Sternberg PW. *Caenorhabditis elegans* inositol 5-phosphatase homolog negatively regulates inositol 1,4,5-triphosphate signaling in ovulation. Mol Biol Cell 2002;13:1641–1651. [PubMed: 12006659]
10. Toker A. The synthesis and cellular roles of phosphatidylinositol 4,5-bisphosphate. Curr Opin Cell Biol 1998;10:254–261. [PubMed: 9561850]
11. Janmey PA. Phosphoinositides and calcium as regulators of cellular actin assembly and disassembly. Annu Rev Physiol 1994;56:169–191. [PubMed: 8010739]
12. Ren XD, Bokoch GM, Traynor-Kaplan A, Jenkins GH, Anderson RA, Schwartz MA. Physical association of the small GTPase Rho with a 68-kDa phosphatidylinositol 4-phosphate 5-kinase in Swiss 3T3 cells. Mol Biol Cell 1996;7:435–442. [PubMed: 8868471]
13. Desrivieres S, Cooke FT, Parker PJ, Hall MN. MSS4, a phosphatidylinositol-4-phosphate 5-kinase required for organization of the actin cytoskeleton in *Saccharomyces cerevisiae*. J Biol Chem 1998;273:15787–15793. [PubMed: 9624178]
14. Boronenkov IV, Anderson RA. The sequence of phosphatidylinositol-4-phosphate 5-kinase defines a novel family of lipid kinases. J Biol Chem 1995;270:2881–2884. [PubMed: 7852364]
15. Desrivieres S, Cooke FT, Morales-Johansson H, Parker PJ, Hall MN. Calmodulin controls organization of the actin cytoskeleton via regulation of phosphatidylinositol (4,5)-bisphosphate synthesis in *Saccharomyces cerevisiae*. Biochem J 2002;366:945–951. [PubMed: 12079494]
16. Hassan BA, Prokopenko SN, Breuer S, Zhang B, Paululat A, Bellen HJ. skittles, a Drosophila phosphatidylinositol 4-phosphate 5-kinase, is required for cell viability, germline development and bristle morphology, but not for neurotransmitter release. Genetics 1998;150:1527–1537. [PubMed: 9832529]
17. Prokopenko SN, He Y, Lu Y, Bellen HJ. Mutations affecting the development of the peripheral nervous system in *Drosophila*: a molecular screen for novel proteins. Genetics 2000;156:1691–1715. [PubMed: 11102367]
18. Weernink PA, Meletiadis K, Hommeltenberg S, Hinz M, Ishihara H, Schmidt M, Jakobs KH. Activation of type I phosphatidylinositol 4-phosphate 5-kinase isoforms by the Rho GTPases, RhoA, Rac1, and Cdc42. J Biol Chem 2004;279:7840–7849. [PubMed: 14681219]
19. Yang SA, Carpenter CL, Abrams CS. Rho and Rho-kinase mediate thrombin-induced phosphatidylinositol 4-phosphate 5-kinase trafficking in platelets. J Biol Chem 2004;279:42331–42336. [PubMed: 15277528]
20. Lee M, Shen B, Schwarzbauer JE, Ahn J, Kwon J. Connections between integrins and Rac GTPase pathways control gonad formation and function in *C. elegans*. Biochim Biophys Acta 2005;1723:248–255. [PubMed: 15716039]
21. Xu X, Rongali SC, Miles JP, Lee KD, Lee M. *pat-4*/ILK and *unc-112*/Mig-2 are required for gonad function in *Caenorhabditis elegans*. Exp Cell Res 2006;312:1475–1483. [PubMed: 16476426]
22. Mello CC, Kramer JM, Stinchcomb D, Ambros V. Efficient gene transfer in *C. elegans*: extrachromosomal maintenance and integration of transforming sequences. EMBO J 1991;10:3959–3970. [PubMed: 1935914]
23. Francis R, Barton MK, Kimble J, Schedl T. gld-1, a tumor suppressor gene required for oocyte development in *Caenorhabditis elegans*. Genetics 1995;139:579–606. [PubMed: 7713419]

24. Francis R, Maine E, Schedl T. Analysis of the multiple roles of gld-1 in germline development: interactions with the sex determination cascade and the glp-1 signaling pathway. Genetics 1995;139:607–630. [PubMed: 7713420]
25. Lee, M. Biology. Iliinois State University; Normal, Illinois: 1997. Characterization of *Caenorhabditis elegans* Extracellular Matrix; p. 125
26. Lee M, Cram EJ, Shen B, Schwarzbauer JE. Role of βpat-3 integrins in development and function of *Caenorhabditis elegans* muscles and gonads. J Biol Chem 2001;276:36404–36410. [PubMed: 11473126]
27. Anderson RA, Boronenkov IV, Doughman SD, Kunz J, Loijens JC. Phosphatidylinositol phosphate kinases, a multifaceted family of signaling enzymes. J Biol Chem 1999;274:9907–9910. [PubMed: 10187762]
28. Kunz J, Wilson MP, Kisseleva M, Hurley JH, Majerus PW, Anderson RA. The activation loop of phosphatidylinositol phosphate kinases determines signaling specificity. Mol Cell 2000;5:1–11. [PubMed: 10678164]
29. Sijen T, Fleenor J, Simmer F, Thijssen KL, Parrish S, Timmons L, Plasterk RH, Fire A. On the role of RNA amplification in dsRNA-triggered gene silencing. Cell 2001;107:465–476. [PubMed: 11719187]
30. Chen N, Harris TW, Antoshechkin I, Bastiani C, Bieri T, Blasiar D, Bradnam K, Canaran P, Chan J, Chen CK, Chen WJ, Cunningham F, Davis P, Kenny E, Kishore R, Lawson D, Lee R, Muller HM, Nakamura C, Pai S, Ozersky P, Petcherski A, Rogers A, Sabo A, Schwarz EM, Van Auken K, Wang Q, Durbin R, Spieth J, Sternberg PW, Stein LD. WormBase: a comprehensive data resource for Caenorhabditis biology and genomics. Nucleic Acids Res 2005;33:D383–389. [PubMed: 15608221]
31. Harris TW, Chen N, Cunningham F, Tello-Ruiz M, Antoshechkin I, Bastiani C, Bieri T, Blasiar D, Bradnam K, Chan J, Chen CK, Chen WJ, Davis P, Kenny E, Kishore R, Lawson D, Lee R, Muller HM, Nakamura C, Ozersky P, Petcherski A, Rogers A, Sabo A, Schwarz EM, Van Auken K, Wang Q, Durbin R, Spieth J, Sternberg PW, Stein LD. WormBase: a multi-species resource for nematode biology and genomics. Nucleic Acids Res 2004;32(Database issue):D411–417. [PubMed: 14681445]
32. Baylis HA, Furuichi T, Yoshikawa F, Mikoshiba K, Sattelle DB. Inositol 1,4,5-trisphosphate receptors are strongly expressed in the nervous system, pharynx, intestine, gonad and excretory cell of *Caenorhabditis elegans* and are encoded by a single gene (*itr-1*). J Mol Biol 1999;294:467–476. [PubMed: 10610772]
33. Ono K, Ono S. Tropomyosin and troponin are required for ovarian contraction in the *Caenorhabditis elegans* reproductive system. Mol Biol Cell 2004;15:2782–2793. [PubMed: 15064356]
34. Berridge MJ, Irvine RF. Inositol phosphates and cell signalling. Nature 1989;341:197–205. [PubMed: 2550825]
35. Berridge MJ, Heslop JP, Irvine RF, Brown KD. Inositol lipids and cell proliferation. Biochem Soc Trans 1985;13:67–71. [PubMed: 2987063]
36. Irvine R. Inositol phospholipids: translocation, translocation, translocation. Curr Biol 1998;8:R557–559. [PubMed: 9707392]
37. Iwasaki K, McCarter J, Francis R, Schedl T. emo-1, a Caenorhabditis elegans Sec61p gamma homologue, is required for oocyte development and ovulation. J Cell Biol 1996;134:699–714. [PubMed: 8707849]
38. Hall DH, Winfrey VP, Blaeuer G, Hoffman LH, Furuta T, Rose KL, Hobert O, Greenstein D. Ultrastructural features of the adult hermaphrodite gonad of *Caenorhabditis elegans*: relations between the germ line and soma. Dev Biol 1999;212:101–123. [PubMed: 10419689]
39. Miller DM, Ortiz I, Berliner GC, Epstein HF. Differential localization of two myosins within nematode thick filaments. Cell 1983;34:477–490. [PubMed: 6352051]
40. Waterston, RH. Muscle. In: Wood, WG., editor. The Nematode *Caenorhabditis elegans*. Cold Spring Harbor Laboratory Press; Cold Spring Harbor, NY: 1988. p. 281-335.
41. Ono K, Yu R, Ono S. Structural components of the non-striated contractile apparatuses in the *Caenorhabditis elegans* gonadal myoepithelial sheath and their essential roles for ovulation. Devel Dyn. 2007In press

42. Rose KL, Winfrey VP, Hoffman LH, Hall DH, Furuta T, Greenstein D. The POU gene ceh-18 promotes gonadal sheath cell differentiation and function required for meiotic maturation and ovulation in Caenorhabditis elegans. Dev Biol 1997;192:59–77. [PubMed: 9405097]
43. Liscovitch M, Chalifa V, Pertile P, Chen CS, Cantley LC. Novel function of phosphatidylinositol 4,5-bisphosphate as a cofactor for brain membrane phospholipase D. J Biol Chem 1994;269:21403–21406. [PubMed: 8063770]
44. Walker DS, Ly S, Lockwood KC, Baylis HA. A direct interaction between IP(3) receptors and myosin II regulates IP(3) signaling in C. elegans. Curr Biol 2002;12:951–956. [PubMed: 12062062]
45. Miller DM, Stockdale FE, Karn J. Immunological identification of the genes encoding the four myosin heavy chain isoforms of Caenorhabditis elegans. Proc Natl Acad Sci U S A 1986;83:2305–2309. [PubMed: 2422655]
46. Strome S. Fluorescence visualization of the distribution of microfilaments in gonads and early embryos of the nematode *Caenorhabditis elegans*. J Cell Biol 1986;103:2241–2252. [PubMed: 3782297]
47. Aono S, Legouis R, Hoose WA, Kemphues KJ. PAR-3 is required for epithelial cell polarity in the distal spermatheca of C. elegans. Development 2004;131:2865–2874. [PubMed: 15151982]
48. Piekny AJ, Johnson JL, Cham GD, Mains PE. The Caenorhabditis elegans nonmuscle myosin genes nmy-1 and nmy-2 function as redundant components of the let-502/Rho-binding kinase and mel-11/myosin phosphatase pathway during embryonic morphogenesis. Development 2003;130:5695–5704. [PubMed: 14522875]
49. Piekny AJ, Mains PE. Rho-binding kinase (LET-502) and myosin phosphatase (MEL-11) regulate cytokinesis in the early Caenorhabditis elegans embryo. J Cell Sci 2002;115:2271–2282. [PubMed: 12006612]
50. Guo S, Kemphues KJ. A non-muscle myosin required for embryonic polarity in Caenorhabditis elegans. Nature 1996;382:455–458. [PubMed: 8684486]
51. Walker DS, Gower NJ, Ly S, Bradley GL, Baylis HA. Regulated disruption of inositol 1,4,5-trisphosphate signaling in Caenorhabditis elegans reveals new functions in feeding and embryogenesis. Mol Biol Cell 2002;13:1329–1337. [PubMed: 11950942]
52. Myers CD, Goh PY, Allen TS, Bucher EA, Bogaert T. Developmental genetic analysis of troponin T mutations in striated and nonstriated muscle cells of Caenorhabditis elegans. J Cell Biol 1996;132:1061–1077. [PubMed: 8601585]
53. Terami H, Williams BD, Kitamura S, Sakube Y, Matsumoto S, Doi S, Obinata T, Kagawa H. Genomic organization, expression, and analysis of the troponin C gene pat-10 of Caenorhabditis elegans. J Cell Biol 1999;146:193–202. [PubMed: 10402470]
54. Kagawa H, Takuwa K, Sakube Y. Mutations and expressions of the tropomyosin gene and the troponin C gene of Caenorhabditis elegans. Cell Struct Funct 1997;22:213–218. [PubMed: 9113409]
55. Cummins C, Anderson P. Regulatory myosin light-chain genes of Caenorhabditis elegans. Mol Cell Biol 1988;8:5339–5349. [PubMed: 3244358]
56. Rushforth AM, White CC, Anderson P. Functions of the Caenorhabditis elegans regulatory myosin light chain genes mlc-1 and mlc-2. Genetics 1998;150:1067–1077. [PubMed: 9799259]

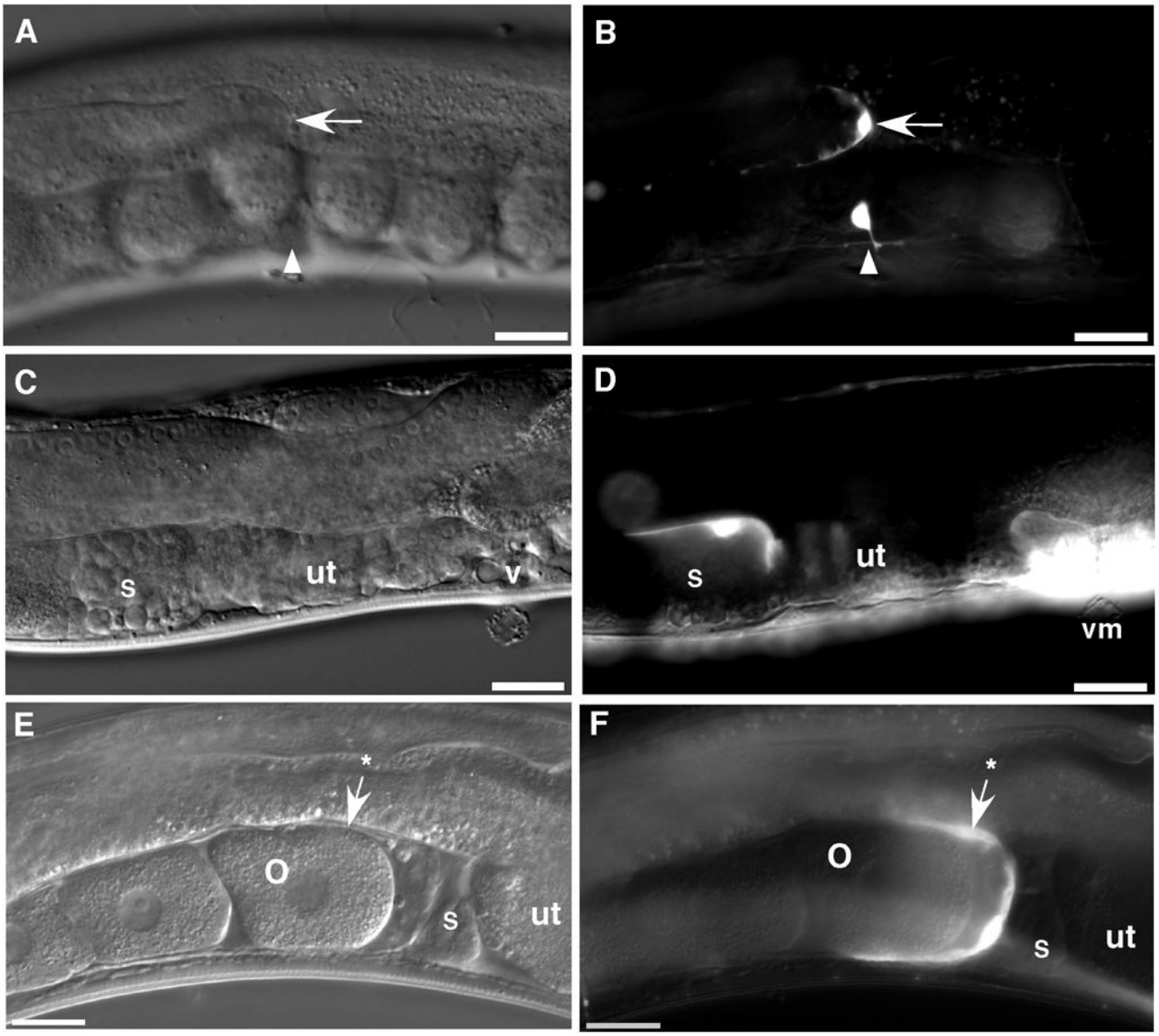

Figure 1. Expression of *ppk-1* in the adult hermaphrodite

ppk-1::GFP transgenic animals were visualized by DIC and fluorescence microscopy. Bright field DIC images (panels A, C, and E) show the mid-body of a representative transgenic *C. elegans* hermaphrodite, including, panel A: distal tip (arrow) of the gonad and ventral mid-body (arrowhead), panel C: spermatheca (s), uterus (ut), and vulva (v), and panel E: oocyte (o), spermatheca (s), and gonad sheath (arrow with an asterisk). Fluorescence images (panels B, D, and E) of the same animals indicate that *ppk-1::*GFP is expressed in the distal tip cell (arrow), ventral neuron (arrowhead), spermatheca (s), vulval muscles (vm), and gonad sheath (arrow with an asterisk). Bars = 20 μm.

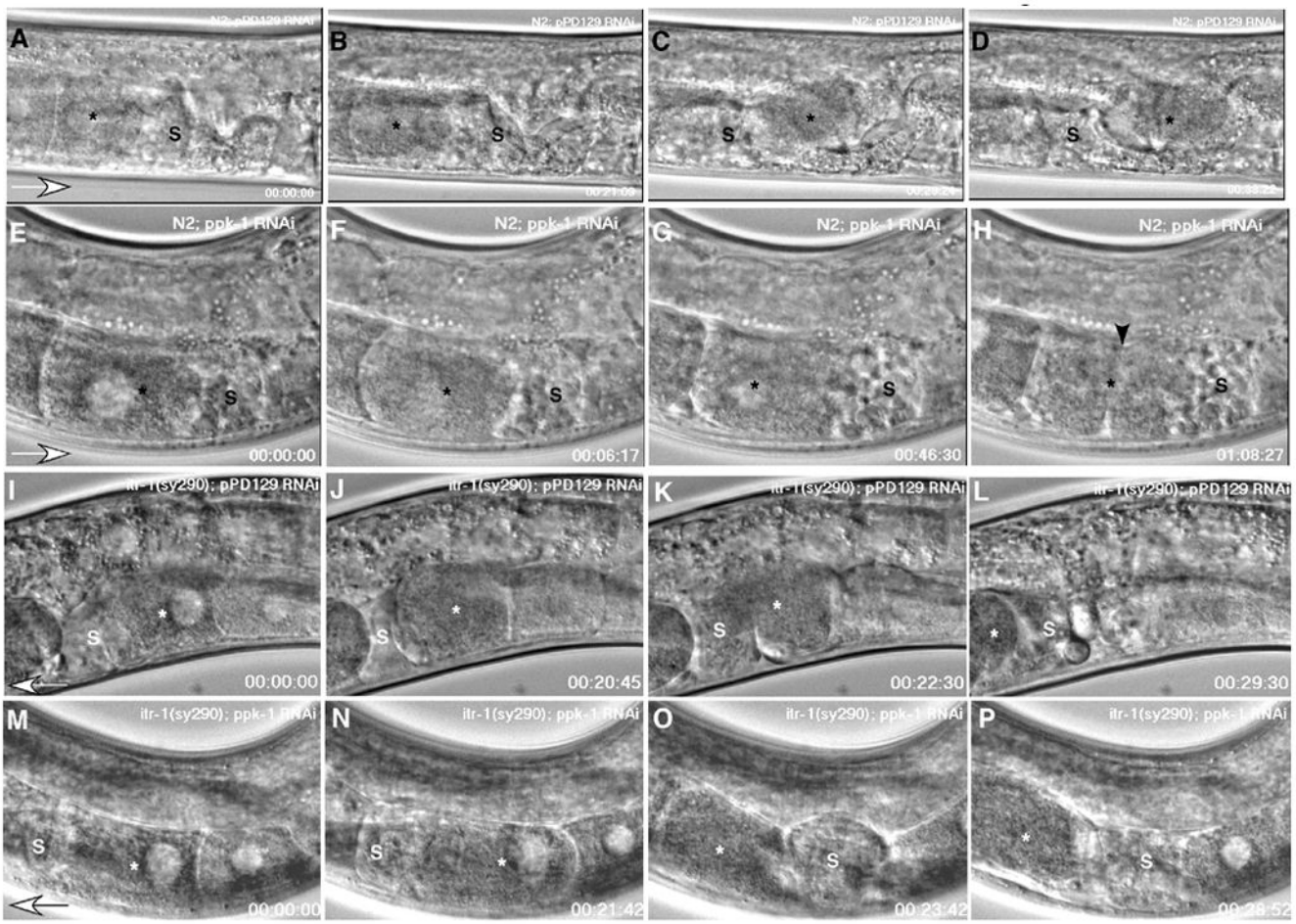

Figure 2. Time-lapse observation of ovulation in *ppk-1* RNAi worms

Panels A – D: N2; control RNAi worms. The oocyte (asterisk) most proximal to the spermatheca (s) undergoes maturation processes such as nuclear envelope breakdown and cell rounding (panel B). Gonad sheath contractions propel the proximal oocyte into the spermatheca for fertilization (panels C and D). Panels E – H: N2; *ppk-1 (RNAi)*. The proximal oocyte (asterisk) also undergoes maturation (panel F). However, it fails to ovulate into the spermatheca due to loss of gonad sheath contraction and spermathecal dilation. Consequently, the nuclear morphology fails to transition (asterisk, panel G), and a cleavage furrow appears following the failed attempt at cell division (arrowhead, panel H). Panels I – L: Gain-of-function *itr-1 (sy290)* suppresses *ppk-1 (RNAi)*. Control RNAi in *itr-1 (sy290)* shows a similar sequence of events in ovulation as N2; control RNAi worms (panels A-D). Panels M – P: Gain of function *itr-1 (sy290); ppk-1 (RNAi)*. The gain in function of *itr*-1 rescues the *ppk*-1 *(RNAi)* phenotype. Ovulation processes progress comparably to those of control RNAi animals in panels A – D and I – L. Open arrowheads indicate the direction of oocyte movement.

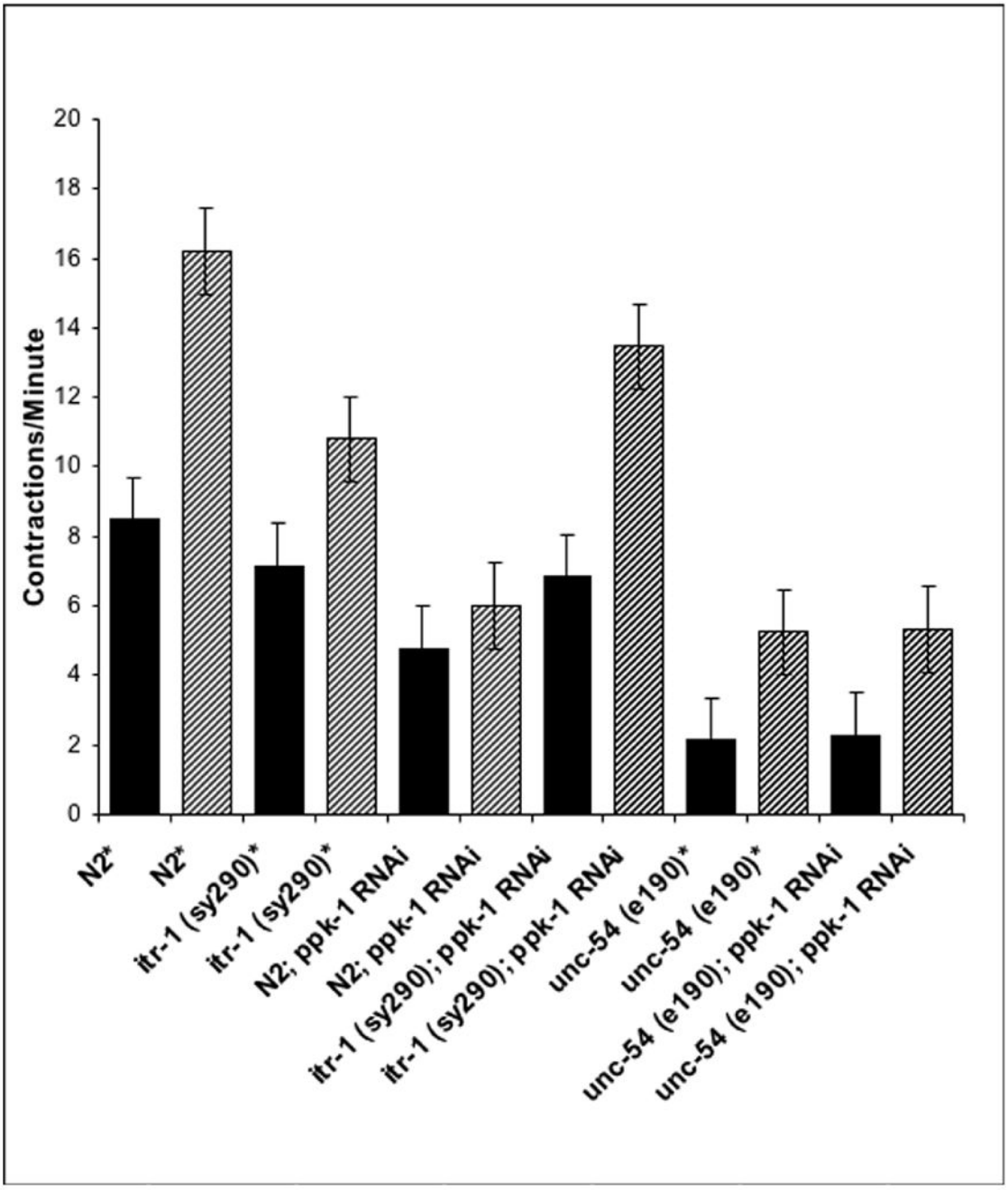

Figure 3. Gonad contractility of *ppk-1 (RNAi)* animals

Using video time lapse DIC video microscopy, gonad contractions were counted for 15 minutes. Solid black bars indicate basal contraction rates; diagonal striped bars indicate ovulatory contraction rates. Samples noted by asterisks were treated with pPD129.26 control bacteria: HT115 *E. coli* transformed with the blank plasmid L4440. Five to six worms were monitored in each experimental group. Error bars indicate standard error of the mean (S. E. M.).

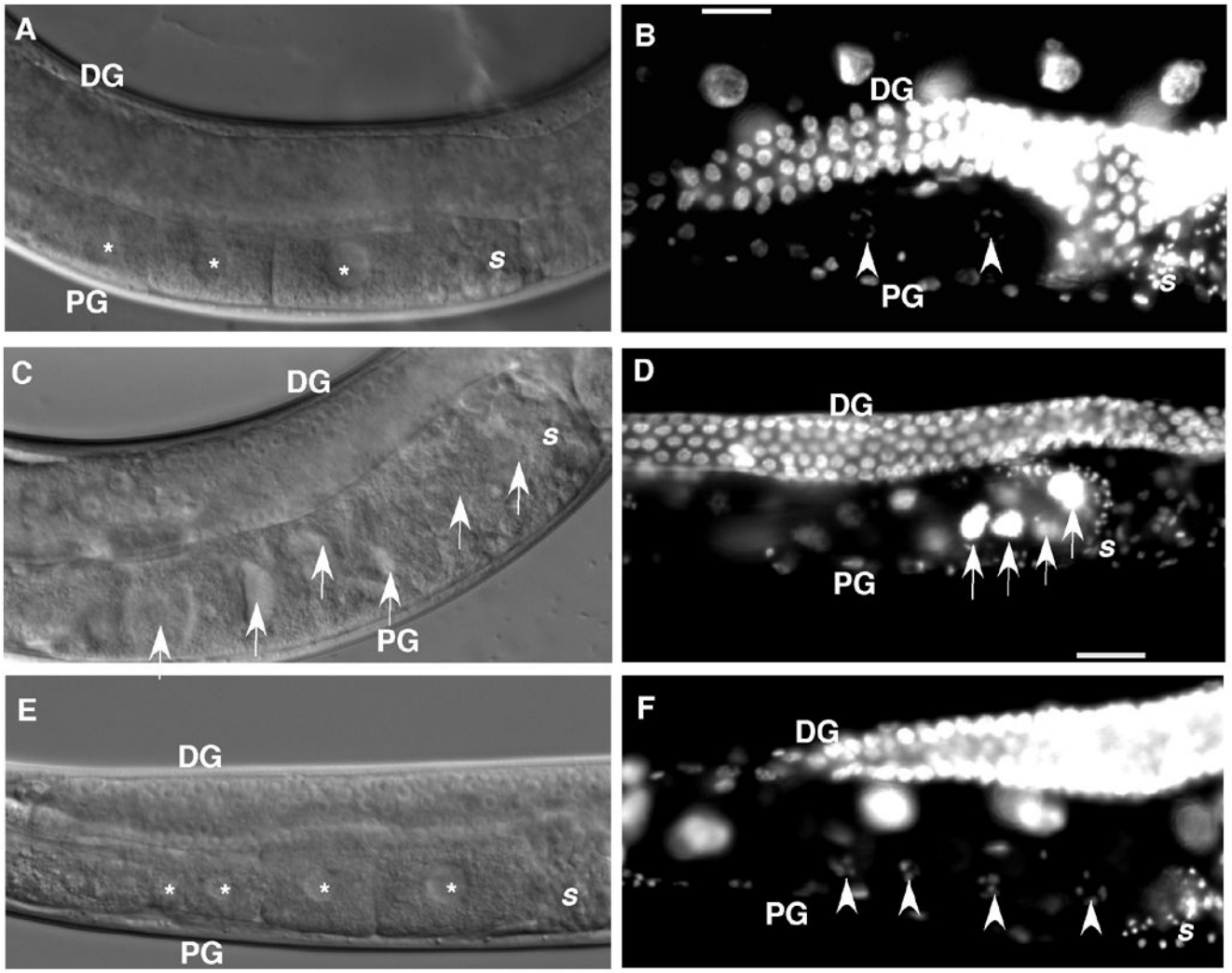

Figure 4. Proximal gonads of *ppk-1 (RNAi)* animals

Panels A, C, and E: DIC microscopy images. Panels B, D, and F: DAPI stained images. Panels A and B: N2; control RNAi worm. A normal assembly line of developing oocytes (panel A, asterisk) in the proximal arm of the gonad (PG) and typical diakinetic oocyte nuclei (panel B, arrowheads) are visualized. Panels C and D: Control N2 worms treated with *ppk-1 (RNAi)*. Oocytes accumulate (arrows) in a non-linear arrangement. The proximal gonad of N2; *ppk-1 (RNAi)* animals is filled with endomitotic (Emo) oocyte nuclei (panel D, arrows). Panels E and F: *ppk-1 (RNAi)* in the *itr-1* (*sy290*) background. The gain-of-function *itr-1* rescues oocyte accumulation. Developing oocytes display a typical linear arrangement (panel E, asterisk) in the proximal gonad. DAPI staining reveals no evidence of Emo oocytes and shows an organized linear arrangement of diakinetic nuclei (panel F, asterisk). DG: distal gonad. PG: proximal gonad. *S*: spermatheca.

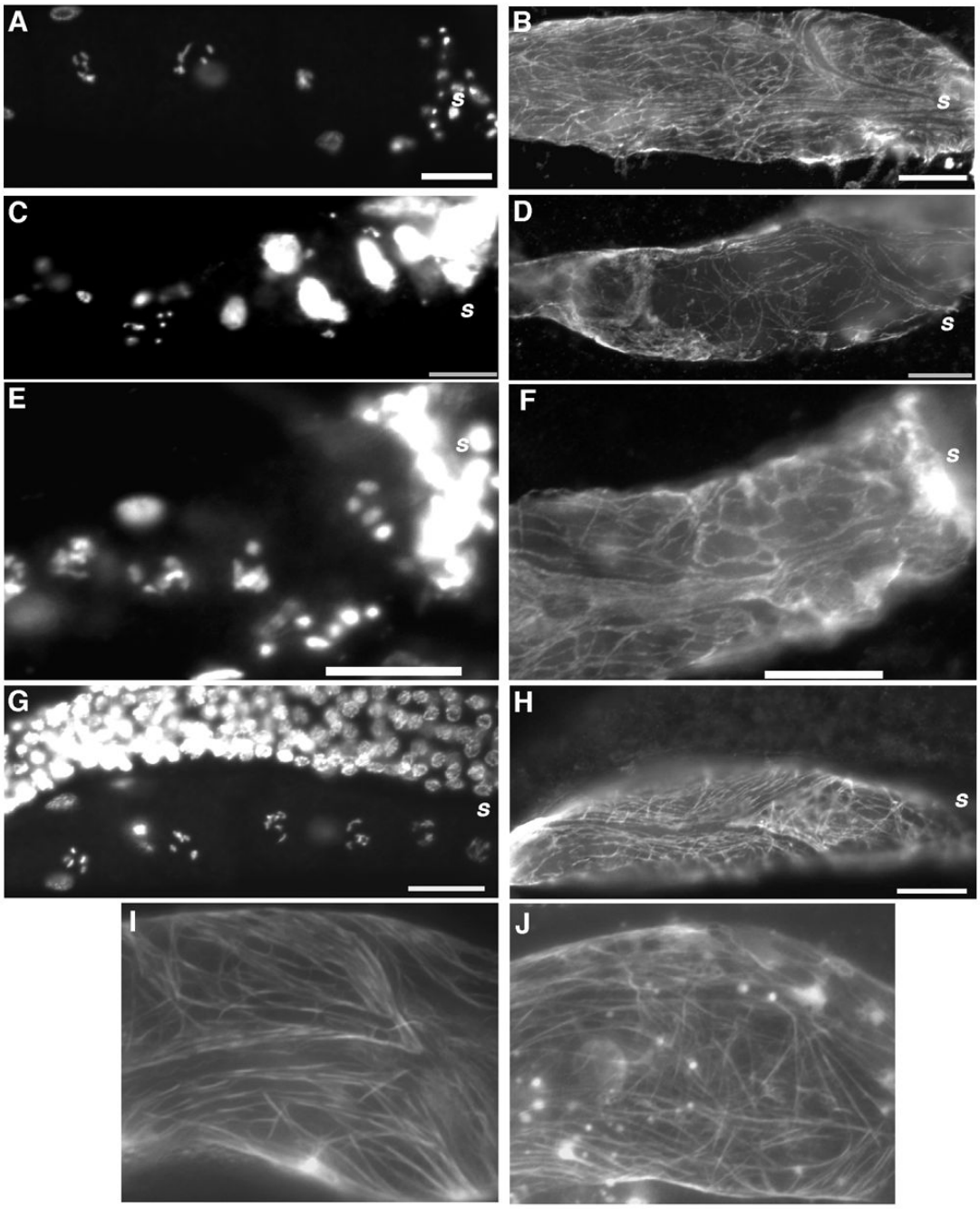

Figure 5. Myosin organization in the proximal gonad of *ppk-1 (RNAi)* animals

Gonad arms of RNAi animals were stained with DAPI (panels A, C, E, and G) and anti-UNC-54/myosin B monoclonal antibodies (panels B, D, F, and H) to visualize nuclear morphology and cytoskeletal myosin in gonad sheath cells. Panels A and B: Control RNAi. The proximal gonad shows typical diakinetic nuclear morphology (panel A) and a randomly but evenly distributed pattern of UNC-54 expression (panel B). Panels C and D: Adult *ppk-1 (RNAi)* in N2 background. The proximal gonad is filled with Emo oocytes (panel C) and patchy myosin filaments (panel D). Panels E and F: L4 or young adult *ppk-1 (RNAi)* in N2 background. These gonads exhibit a DAPI staining pattern with some normal punctuate patterns (panel E, compare to panels A and C), but show less organized myosin distribution than those of control

RNAi (compare to panel B), resembling the staining pattern in the adult stage *ppk-1 (RNAi)* worms (compare to panel D). Panels G and H: *ppk-1 (RNAi); itr-1 (sy290)*. Defects resulting from *ppk-1 (RNAi)* are suppressed in the *itr-1 (gf)* background. Panels I and J: A GFP fusion transgene confirms cytoskeletal distribution data. To verify the cytoskeleton distribution at the stage of L4 or young adult stage, transgenic worms expressing *pat-10*/Troponin C::GFP driven by the *ppk-1* promoter in gonad sheath cells were subjected to *ppk-1 (RNAi)* and stained with anti-UNC-54/myosin B antibody. Control RNAi (panel I) shows a well-organized cytoskeleton pattern, whereas the gonad sheath of *ppk-1 (RNAi)* (panel J) shows more perpendicular filaments and generally less organization than the control RNAi animals (panel I). Bars = 20 μm.

Table 1

Sterility of *ppk-1 (RNAi)* animals

Strains	% Sterile (*N*)
N2; *ppk-1 (RNAi)*	93 ± 3 (100)
rrf-1 (*pk1417*); *ppk-1 (RNAi)*	0 (55)
N2*	0 (40)
itr-1/lfe-1 (*sy290*); *ppk-1 (RNAi)*	2.5 ± 2 (77)
itr-1/lfe-1 (*sy290*)*	0 (40)
lfe-2 (*sy326*); *ppk-1 (RNAi)*	75 ± 2 (88)
lfe-2 (*sy326*)*	0 (40)
ipp-5 (*sy605*); *ppk-1 (RNAi)*	62 ± 2 (50)
ipp-5 (*sy605*)*	0 (30)
unc-54 (e190); *ppk-1 (RNAi)*	88 ± 4 (65)
*unc-54 (e190)**	20 ± 6 (40)

N = number of animals. Each data entry represents the sum of at least 2–3 phenotypic scorings. The errors indicated in parentheses represent the standard error of the mean.

* Tested on pPD129.36 control bacteria: HT115 *E. coli* transformed with the empty plasmid L4440.

Table 2

Examination of the ovulation process by time-lapse recording

Strain	RNAi	Sheath Contract	Sperm. Dilation	Oocyte maturation*	Aberrant cytokin.	Ovul.	N
N2	control	100	100	100	0	100	9
N2	*ppk-1*	100	0	100	100	0	10
itr-1 (sy290)	control	100	100	90	0	100	10
itr-1 (sy290)	*ppk-1*	100	100	80	0	100	8
ipp-5 (sy605)	control	100	100	100	0	100	6
ipp-5 (sy605)	*ppk-1*	100	66	100	33	66	6
unc-54 (e190)	control	100	66	100	33.3	66.6	6
unc-54 (e190)	*ppk-1*	100	0	100	100	0	6

*Nuclear disappearance and cell rounding of an oocyte were scored as maturation.

**All values except column ‘N’ indicate percentage. Column ‘N’ indicates the number of worms observed.